Ultrasonics - Sonochemistry 51 (2019) 197–205

Contents lists available at ScienceDirect

Ultrasonics - Sonochemistry

journal homepage: www.elsevier.com/locate/ultson

Performance of SiO_2/Ag Core/Shell particles in sonocatalalytic degradation of Rhodamine B

İlyas Deveci[a,*], Bedrettin Mercimek[b]

[a] Konya Technical University, Vocational School of Technical Sciences, Chemistry and Chemical Processing Technologies, Konya, Turkey
[b] Necmettin Erbakan University, Ahmet Kelesoglu Faculty of Educational Sciences, Department of Mathematics and Science Education, Konya, Turkey

ARTICLE INFO

Keywords:
Sonocatalytic degradation
SiO_2/Ag Core/Shell nanoparticles
Rhodamine B
Ultrasonic irradiation

ABSTRACT

In this study, SiO_2/Ag Core/Shell nanoparticles was prepared and sonocatalytic activity of prepared catalyst was investigated by using Rhodamine B as model contaminant, at 35 kHz using ultrasonic power of 160 W within 90 min. The change in efficiency in the sonocatalytic degradation of Rhodamine B catalyzed by SiO_2/Ag Core/Shell nanoparticles with respect to the initial concentration of dye, catalyst amount and temperature were firstly investigated. Optimal conditions were found as follows: catalyst amount = 15 mg/L, Temperature = 25 °C and initial concentration of dye = 10 ppm. Influence factors such as pH of solution, O_2 saturation of solution and the concentration of H_2O_2 added to the solution, on degradation efficiency in presence of catalyst, were investigated. SiO_2/Ag Core/Shell nanoparticles showed higher sonocatalytic activity at pH = 7 with respect to acidic and alkaline conditions. Degradation efficiency was reached up to 67% in experiments which air pumped (0.6 L/min) through the solution with in 90 min. It was observed that the dye removal increased via increase while H_2O_2 concentration lower than 10 mM. Higher concentration of H_2O_2 than the optimal concentration had adverse effect on degradation efficiency. Our results showed that the SiO_2/Ag Core/Shell nanoparticles were active catalyst for sonocatalytic degradation of dyes. Reusability of the catalyst was investigated.

1. Introduction

Water pollution is one of the major issues to be resolved around the world because of its versatile, harmful effects on human health and the environment. Especially, coloured wastewater could be the dominant pollutant in industrial area [1]. Beside the unaesthetic vision of colored effluents, they decrease the penetration of sun light into water reservoirs and so it has destructive effect on photosynthesis in aquatic flora [1,2]. Furthermore, deposition and anaerobic decomposition of these effluents could produce hazardous secondary contaminants that causes water and soil pollution [3]. Colored waste water is formed in many industries such as textile, cosmetic, leather and paper. Discharging of effluents is controlled by environmental regulations and disposal of them is not allowed without appropriate treatment. There are several treatment methods that recommended for degradation of organic pollutants in wastewater such as adsorption, Fenton reactions, photocatalytic oxidation, ozonation, electro catalytic oxidation. Use of combination of these methods and use of oxidative chemicals (H_2O_2, NaOCl etc.) in these methods discussed in literature before [4–6]. Each of them has their own specific advantages and disadvantages. Degradation of organic contaminates by using sonolytic and sonocatalytic oxidation in aqueous media is another promising approach in last decades. Ultrasonic sound wave is main driven force in these methods.

Ultrasound is sound wave which has frequencies in ranges between 18 kHz and 10 MHz. When ultrasound is applied in liquid media, it causes acoustic cavitation. Acoustic cavitation is phenomenon described as formation, growth, and collapse of microbubbles in liquid media in very short period. During the collapse of microbubbles filled with vapor and dissolved gas in liquid, some physical effects such as microjets, turbulence, shock waves, share forces etc., are formed. Breaking down of the microbubbles produces local hot spots. These hot spots could reach the temperatures up to 5000 K and pressure higher than 1000 atm [7,8] Because of these extreme conditions organic molecules could be destructed directly or decomposed with the radicals ($–OH^-$, $–OOH^-$ etc.) formed during the collapse of the microbubbles [8]. Unfortunately, using power ultrasound for destruction of organic contaminant in waste water consumes lots of energy and reaction rate of the decomposition is too low [9,10]. To overcome these problems several affords such as using various type of catalyst and using oxidative reagents, was devoted in literature. Heterogeneous catalysts could be preferable because they could be easily separated from liquid media and they don't cause secondary contaminations. Interface between

* Corresponding author.
E-mail addresses: ideveci@selcuk.edu.tr (İ. Deveci), bmercimek@konya.edu.tr (B. Mercimek).

https://doi.org/10.1016/j.ultsonch.2018.10.025
Received 5 September 2018; Received in revised form 9 October 2018; Accepted 17 October 2018
Available online 19 October 2018

heterogeneous catalyst and water produces weak points that could promote the formation of cavitation bubbles thus increase the degradation rate of direct and indirect oxidation of organic molecules in water. On the other hand, using high amount of catalyst could have adverse effect on degradation rate of contaminants, by the way of scattering of ultrasound waves and mutual screening effects [11].

Various type of heterogeneous catalyst such as metal oxides (TiO_2, ZnO [6] and CuO [12]), modified TiO_2 (Au/TiO_2 [13], Cr/TiO_2, Co/TiO_2 [14], CdS/TiO_2 core-shell [15]), solid acid catalyst ($H_3PW_{12}O_{40}$/ZrO_2 [16]) etc. were used for degradation of contaminants in water. Also effect of the size of the catalyst on sonocatalytic degradation rate was examined in literature [17]. In last decades, nanomaterials are attracting too much attention because of unique properties distinctly different with respect to their bulk form. At nanometer scale, beside the increases in surface area of the materials, the other properties such as reactivity, strength, electrical and magnetic properties are also improved [18]. Nanoparticles and nanocomposites have been used in many applications [19,20], At the point of modification of nanomaterials with active sites, the supporting nanomaterial can supply excellent advantages such as high surface area, low mass transfer resistance and high particle mobility [15,21]. Recently, Silver nanoparticles and nanocomposites attract too much attention the for catalytic applications, especially in degradation of dye effluents [22]. It was reported that, Silver nanoparticles has role as redox catalyst by the way of electron relay effect [23]. Also, it was reported that, the silver nanoparticles improve oxidative degradation efficiency by the Fenton like process with H_2O_2 [24]. On the other hand, the size of the particle is limiting factor for using them for environmental application because of separation problem. In some cases, the nanoparticles is not separated from the solution and it causes additional contamination. In the case of Silver nanoparticles, it was reported that it was poisonous to some aquatic organisms [25]. To overcome these disadvantages, integration of nanoparticles to another surface could be the solution.

Beside the use of ultrasound in degradation of dyes, sonochemical approach was extensively used in preparation of nanoparticles and nanocomposites [26,27]. Shock waves formed during the ultrasonic cavitation may cause interparticle collisions which the velocities of hundreds of meters per second. These high energetic impacts lead to changes in characteristic properties of the prepared particles such as particle size distribution, texture and surface compositions [28,29]. In this study ultrasound was used for both degradation of dyes and preparation of SiO_2 nanoparticles. Using ultrasound for preparation of SiO_2 could improve the homogeneity in size distribution and prevent aggregation of obtained particles.

In this study, SiO_2/Ag Core/Shell nanoparticles which were thought as appropriate catalyst for sonocatalytic oxidation of organic pollutants found in wastewater were synthesized. In literature, there were several reports on preparation of silver nanoparticles and nanocomposites by using both biosynthesis and sonochemical route [30,31]. SiO_2/Ag Core/Shell nanoparticles was used as sonocatalyst for the first time in this study. For preparation SiO_2/Ag Core/Shell nanoparticles, firstly silica particles was synthesized, and then the surface of the particles was tailored with Ag nanoparticles. Obtained SiO_2/Ag Core/Shell nanoparticles characterized by using XRD, SEM, TEM, FTIR-ATR and N_2 adsorption, techniques. Rhodamine-B was used as a model contaminant. Influence factors for the sonocatalytic degradation of dye stuff: catalysis amount (5 mg/L, 10 mg/L, 15 mg/L, 20 mg/L and 30 mg/L), the initial concentration of the dye solution (5 ppm, 10 ppm, 20 ppm and 40 ppm), temperature (25, 35 and 45° C), pH (4, 7 and 9), the H_2O_2 concentration (1, 5, 10, 20, 30, 40 and 50 mM) and O_2 saturation (0.6 L/min air) were examined. Sonocatalytic oxidation experiments was performed in batch system by sampling in different time intervals.

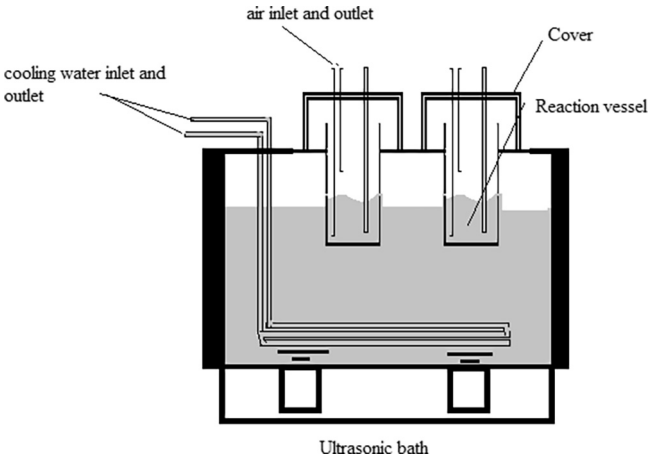

Fig. 1. Experimental Setup.

2. Experimental

2.1. Materials

In this study, Tetraethyl orthosilicate (TEOS) (99% Aldrich), ethanol (98.9% Aldrich), ammonium hydroxide (28% MERCK), $AgNO_3$ (Aldrich, 99%), (3-Mercaptopropyl) trimethoxysilane (95%, Aldrich) and $NaBH_4$ (≥98.0% Aldrich) were used for synthesis of SiO_2/TiO_2 and SiO_2/Ag Core/Shell nanoparticles. Rhodamine-B (Rh-B) (≥95%) purchased from SIGMA was used as model contaminant.

2.2. Apparatus and experimental procedure

The experimental setup used in this study is shown in Fig. 1. The sonocatalytic degradation experiment was performed by using an ultrasonic bath (Bandelin electronic RK 255H, Germany) at 35 kHz and 160 W. The temperature of the reaction was controlled with water circulation.

In a typical experimental run, firstly appropriate amount of catalyst was dispersed in pure water and then required amount of Rh-B (200 ppm stock solution) was added into the dispersion. The mixture was stirred for an hour to adjust the adsorption equilibrium. At the end of this period, the ultrasound power source was turned on and 2 ml aliquots were pipetted for certain time interval. Pipetted aliquots were centrifuged at 10 000 rpm and analyzed by using UV–Vis. Firstly, to optimize reaction conditions, the effect of initial dye concentration (5, 10, 20 and 30 ppm), effect of catalyst loading (5 mg/L, 10 mg/L, 15 mg/L, 20 mg/L and 30 mg/L) and effect of temperature on degradation efficiency were investigated. To investigate effect of pH of solution on removal of Rh-B, experiments were performed under three different pH (4, 7 and 9). pH of the solution was adjusted by using HCl (0.1 M) and NaOH (0.1 M) solution. In this study, the effect of H_2O_2 addition on degradation rate was also investigated. For this purpose, different amount of H_2O_2 solution (1 M) was added into the reaction medium just before the beginning of the experiment to adjust the concentration of H_2O_2 in final solution (1, 5, 10, 20, 30, 40 and 50 mM). To investigate the effect of O_2 saturation of the solution on degradation efficiency, air was pumped into the reaction medium with the rate of 0.6 L/min. For all experimental run, degradation efficiencies of Rh-B dye were calculated according to the following equation:

$$Rh\_B\ deg.\ eff.\ (\%) = \left(1 - \frac{Abs_t\ (554\ nm)}{Abs_0\ (554\ nm)}\right) * 100 \quad (1)$$

where, Abs_t (554 nm) is the absorbance value of Rh-B dye at 554 nm at time t and Abs_0 (554 nm) is the initial absorbance value of Rh-B solution. Each experiment was repeated, and mean values of the results

were taken into consideration.

2.3. Preparation of SiO_2 nanoparticles

The uniform-sized SiO_2 nanoparticles were prepared by the method described in the literature [32] with little modifications. Water was added into ethyl alcohol as the total volume of the solution was 50 ml. The solution was then left in the ultrasonic bath for 10 min. The TEOS was rapidly added to the solution environment and the solution was left in the ultrasonic bath for 30 min. After this period, required amount of ammonium hydroxide (28%) was added into the solution and sonicated for an hour. Molar ratio of the TEOS/NH_4OH/H_2O/Ethyl Alcohol was kept as 1/3.3/40/162.7 in final solution. Then, the resulting cloudy solution was stirred at room temperature for 16 h. The finally obtained particles were washed with pure water and ethyl alcohol until pH = 7.

2.4. Preparation of SiO_2/Ag Core/Shell nanoparticles

The method used for preparing SiO_2/Ag Core/Shell nanoparticles is as follows. Firstly, the surface of the SiO_2 particles was modified by using the (3-mercaptopropyl) trimethoxysilane. For this purpose, 1.5 g of SiO_2 particles was dispersed in 30 ml of dry toluene, then 1.5 ml (3-mercaptopropyl) trimethoxysilane was added into suspension and refluxed for 24 h in nitrogen atmosphere. The resulting structure was separated from the toluene by centrifugation and washed with dry acetone, ethyl alcohol and diethylether, respectively, to remove the unreacted (3-mercaptopropyl) trimethoxysilane. 0.5 g of modified SiO_2 particles was dispersed in 30 ml of ethanol and water mixture (5/1:v/v). 0.01 g of $AgNO_3$ was added into the suspension and stirred for 30 min. Then ice cold 10 ml of $NaBH_4$ solution (0.132 g in 10 ml water) was added dropwise into the suspension. The resulting mixture was stirred for 16 h. The resulting particles was separated by centrifugation, washed several times with water, dried at 110 °C and calcined at 550 °C.

2.5. Characterization of catalyst

The crystal structures of the obtained particles were investigated by using X-Ray Diffractometer (Rigaku, SmartLab). The crystallographic structure of the catalysts was determined at a rate of 3.75 deg./min and in the range of 2θ = 5–80°. The textural properties of prepared particles (Brunauer–Emmett–Teller surface areas (S_{BET})), Average pore size and total pore volume) were investigated by N_2 adsorption at 77 K using sorptometer (Micromeritics, Gemini V2.01). Morphology and the size of the prepared catalyst were investigated by using Scanning Electron Microscope (JEOL – JSM-7600F) with different magnification. Transmission Electron Microscope (TEM) images were recorded by using JEOL JEM-2100 (UHR). Metal content was determined by using SEM-EDX (JEOL – JSM-7600F). IR spectrums of the catalyst were recorded by using FT-IR spectrometer (Nicolet IS-10) with ATR attachment.

3. Results and discussion

3.1. Characterization of catalyst

XRD was used to evaluate the phase structure of Ag coated on SiO_2 particles. Clear peaks were observed on SiO_2/Ag Core/Shell nanoparticles, which were not observed in the support materials. These peaks belong to metallic states of the Ag that make up the shell structure. XRD patterns of SiO_2 nanoparticles and SiO_2/Ag Core/Shell particles are shown in Fig. 2. As seen in Fig. 2, there was only diffuse peak located at 2θ = 16–30° was observed for the uncoated SiO_2 particles. This result indicate that the obtained SiO_2 particles were in amorphous form.

The XRD spectrum of the SiO_2 microspheres loaded with Ag is shown in Fig. 2. In the obtained spectrum, peaks located at 2θ = 38.1, 44.32, 64.34 and 77.49 arising from metal loading were observed. These peaks were thought to originate from the reflections of the (1 1 1), (2 0 0), (2 2 0) and (3 1 1) planes of the face-centered cubic (FCC) silver crystal. The obtained results were in agreement with the standard spectrum of the silver crystals (JCPDS file no. 04-0783) and literature [33]. The particle size of the Ag crystals on silica surface was determined as 29.9 nm by using the Scherrer equation. Equation (2) shows the Scherrer equation. In the equation, λ is the wavelength of the X-rays, β is the peak width in half of the maximum peak length (FWHM), and θ is the angle at which the most intense peak is seen.

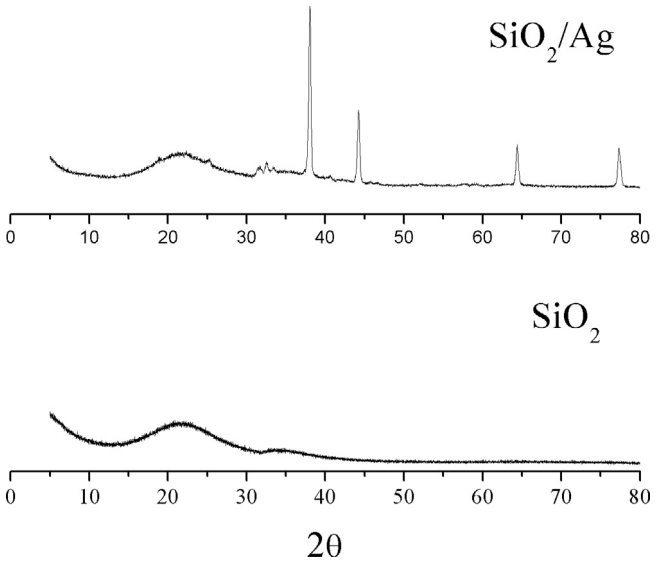

Fig. 2. XRD patterns for prepared SiO_2/Ag Core/Shell nanoparticles and SiO_2 nanoparticles.

$$d = \frac{0.9 \times \lambda}{\beta cos(\theta)} \quad (2)$$

Textural properties of prepared SiO_2 nanoparticles and SiO_2/Ag Core/Shell nanoparticles are reported in Table 1. As seen in Table 1 the surface area of SiO_2/Ag Core/Shell nanoparticles much higher than that of SiO_2 nanoparticles. The average pore diameter of SiO_2/Ag Core/Shell particles increased 6-fold with respect to that of SiO_2 particles. Also, mean pore volume of Ag loaded sample increased. Fig. 3 shows SEM images and EDX spectra of prepared catalyst (a) SiO_2 and (b) SiO_2/Ag Core/Shell nanoparticles. As seen in figures, it has been observed that SiO_2 nanoparticles (Fig. 3a) had smooth surface. This observation showed that the structure was non-porous. The same feature was also observed in N_2-Ads studies (Table 1). SiO_2 nanoparticles had spherical shape and the size of the SiO_2 nanoparticles were varying between 490 and 630 nm. It was observed that there was no agglomeration of SiO_2 particle. It was reported that using ultrasound avoided the particle agglomeration [34]. After metal loading, as seen in Fig. 3b accumulations were easily seen on SiO_2 nanoparticles. In addition to that, there was no metal aggregate observed in obtained SEM images. This result indicated that the accumulation of material was homogeneous, and the surface of SiO_2 nanoparticles appear to be covered with the Ag particles. The particle diameters of SiO_2/Ag Core/Shell nanoparticles were

Table 1
Textural properties of synthesized catalysis systems.

Sample	S_{BET} (m^2/g)	Total Pore Volume (cm^3/g)	Mean Pore Volume (nm)
SiO_2 nanoparticles	7.5	0.011	9.27
SiO_2/Ag Core/Shell nanoparticles	18.4	0.064	13.23

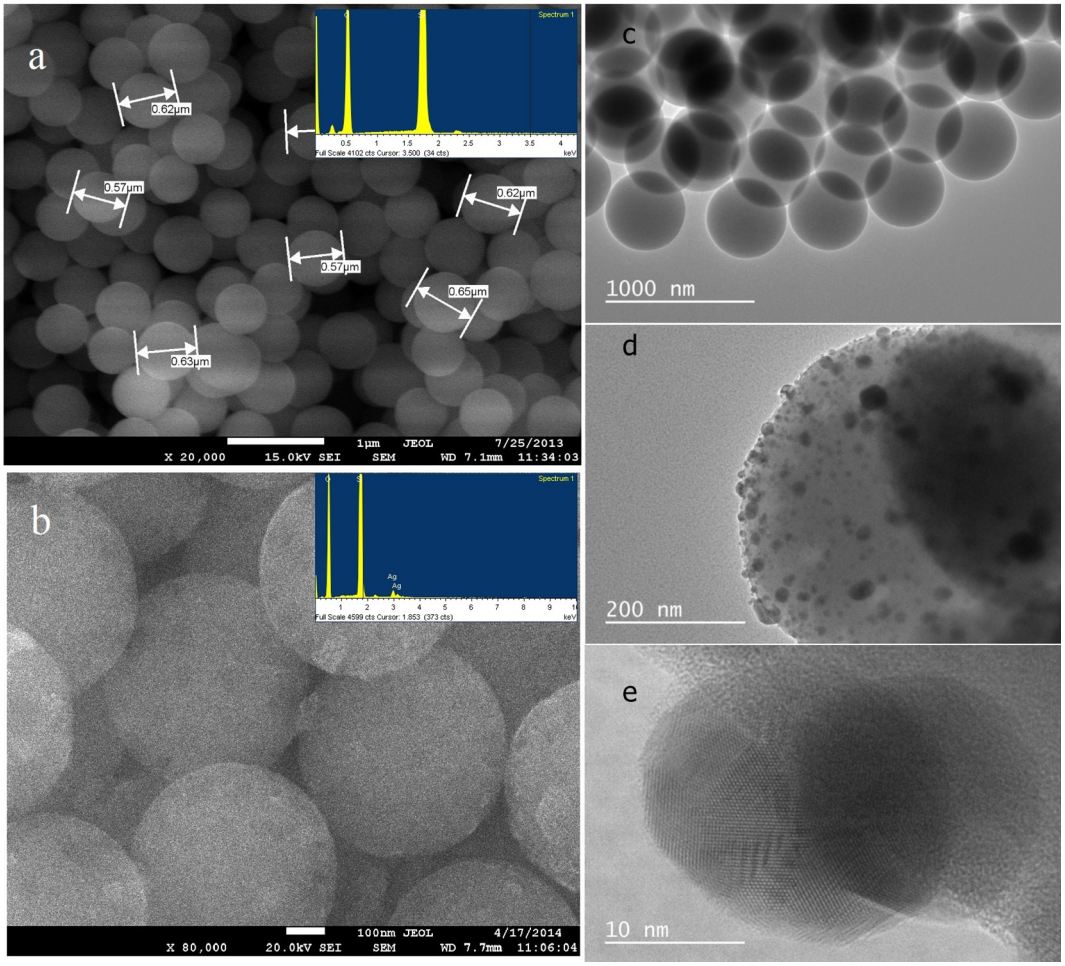

Fig. 3. SEM images of SiO_2 nanoparticles (a), SiO_2/Ag Core/Shell nanoparticles (b) (inset figure shows the EDX spectrum of the particles), TEM images of SiO_2 nanoparticles (c), SiO_2/Ag Core/Shell nanoparticles (d), Ag crystal on SiO_2 surface (e).

varying between 521 and 569 nm. Inset figures shows the EDX spectrum of the prepared particles. EDX results indicated that the amount of Ag deposited on the surface of the was determined as 4.94%. TEM images of SiO_2 nanoparticles and SiO_2/Ag Core/Shell nanoparticles are shown in Fig. 3(c) and (d), respectively. For the uncoated particles as seen in Fig. 3(c), In agreement with the SEM analysis, all the particles had smooth texture and perfect spherical shape. In the figure, all the particles were nearly equidimensional. The average diameter of SiO_2 nanoparticles were found as 527 ± 7 nm. In Fig. 3(d), accumulation of Ag nanoparticles on surface was observed. The obtained SiO_2/Ag Core/Shell nanoparticles were close to spherical in shape and same with the uncoated samples, homogenous size distribution was observed. The average diameter of the SiO_2/Ag Core/Shell nanoparticles was found as 498 ± 19 nm. Interestingly, it was found that the average size of the SiO_2/Ag Core/Shell nanoparticles was lower than that of uncoated samples. Shrinkage of the particles may arise from the condensation of silanol group into silica during the calcination of SiO_2/Ag Core/Shell nanoparticles. The single Ag crystal incorporated onto surface was seen in Fig. 3(e). The crystalline nature of the particles seen in figure. The size of Ag nanoparticles on the surface was varying between 3 and 42 nm. In agreement with the XRD studies, mean width of the particles was found as 21.2 ± 9 nm.

Fig. 4a shows ATR-FTIR spectrum of SiO_2 nanoparticles and SiO_2/Ag Core/Shell nanoparticles. Fig. 4b shows FTIR spectrum of SiO_2 nanoparticles and (3-mercaptopropyl) trimethoxysilane modified SiO_2 nanoparticles (SiO_2-S). FTIR spectrum of SiO_2 nanoparticles and SiO_2-S was obtained by using KBr pallets (1 mg sample and 100 mg KBr). In

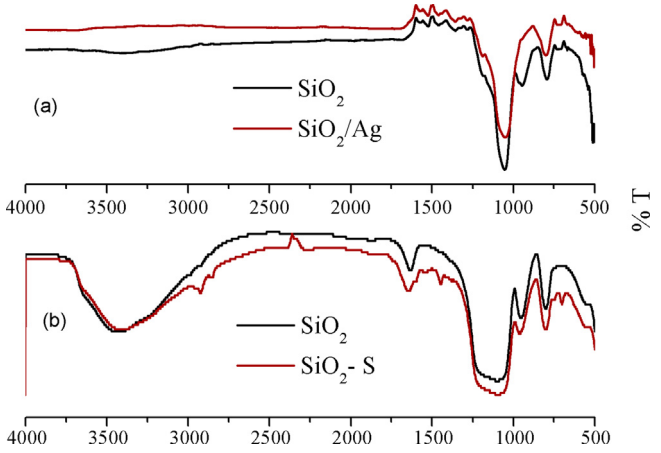

Fig. 4. ATR-FTIR spectrum of SiO_2 nanoparticles and SiO_2/Ag Core/Shell nanoparticles (a), FTIR spectrum of SiO_2 nanoparticles and (3-mercaptopropyl) trimethoxysilane modified SiO_2 nanoparticles (b).

Fig. 4b, it was observed that there were peaks at 2924 and 2852 cm^{-1}, in addition to the structural peaks of the support structure. These peaks are described in the literature as symmetric and asymmetric stretching peaks of ($–CH_2$) groups. It was thought that these peaks belong to, $–CH_2$ functional groups of (3-Mercaptopropyl) trimethoxysilane structure, and surface modification studies was successfully carried out. It was reported that affinity of the –OH and –SH groups toward Ag+ ions were

different and, the interest of –SH groups against Ag + ions much higher than that of –OH groups. Also it was reported that the –SH groups fixation on the surface was necessity for the Ag shell formation [35]. It is also pointed out in the literature that, there were large broad peak, at around 3400 cm^{-1}, belonging to asymmetric stretching of –OH group originating from silanol groups. The decrease in intensity of this peak with respect to that of other structural peak showed that, some of –OH group was consumed during the surface modification. These results indicate that –SH groups successfully inserted onto SiO_2 nanoparticle surface. As seen in Fig. 4a, after reduction of Ag^+ ion on the surface, the structural peaks, except for the peak at 944 cm^{-1} belonging to Si-OH symmetrical stretching, were preserved. This could be arisen from the condensation Si-OH into SiO_2 during the calcination process.

3.2. Catalytic activity results

There are many factors that affect the sonocatalytic degradation of the dyes. Reaction temperature, pH, amount of catalyst, initial dye concentration, and oxygen saturation of the reaction solution are factors that influence the reaction yield. To determine the activities of prepared catalysts appropriately, optimum reaction conditions must first be determined. Optimum reaction conditions depend on the frequency of the ultrasound source used, the type of ultrasonic source used, the size of the catalyst used, the nature of the dye and many other parameters. Firstly, effect of system parameters such as temperature, amount of catalyst and initial dye concentration on degradation efficiency, were investigated. The results are shown in Fig. 5. Fig. 5(a) shows the Rh-B degradation efficiency at the end of 90 min for 4 different initial concentrations and the other parameters were kept constant. As seen in figure, it was found that initial dye concentration was inversely proportional with the degradation efficiency. Same observation was obtained in literature. Wang and colleagues examined the removal of Rh- B and Acid Red at various starting concentrations using ZnO nanoparticles. Parallel to our results, they observed reduction in the rate of degradation efficiency despite increased dye concentrations. The reduction in degradation efficiency was explained by the fact that the dye molecules covered the surface of the particles and prevented ·OH radicals from adsorbing on the catalyst surface [36]. In Fig. 5(b), the effect of catalyst amount on degradation efficiency is shown. The maximum degradation efficiency was obtained in experiment which the catalyst amount set at 15 mg/L. In general, the increase in the amount of catalyst, increases the number of molecules adsorbed to the surface, increases the number of radicals formed due to the number of cavitation bubbles formed, thereby increase the degradation efficiency. But as reported in literature, there are certain limitations on the rising the amount of catalyst. The usage of catalyst over the optimum amount causes the scattering of ultrasound waves, in solution, resulting in a reduction in degradation efficiency [11]. In order to investigate the change in Rh-B degradation efficiency at different temperatures, experiments were carried out by varying the solution temperature while keeping all other parameters constant. Corresponding results are shown in Fig. 5(c). As seen in figure, degradation efficiency decreased with the increasing of reaction temperature. Studies in which the effect of temperature is examined in the literature have different results. In the literature, due to the increase in vapor pressure, the liquid can evaporate more easily and reduce the maximum heat obtained during the collision of cavitation bubble, although the temperature causes more cavitation bubbles because the temperature reduces viscosity, surface tension and gas solubility. Therefore, the amount of radical formation and the degradation efficiency decrease. But, as in the case of conventional reactions, the temperature increases the rate of reaction because it increases the number of reactants that can perform effective collisions [37]. The factors mentioned above, had positive and negative effect on degradation efficiency. Superiority of the effects depended on the mechanism of reaction. In the case of our study it was thought that the increase in temperature might lead to lower temperature achieved during the collision of cavitation bubble, decreased the adsorption of radicals on surface and degassing of the solution. So, increase of temperature decrease the degradation efficiency. Same observations were obtained in literature [38]. Optimum parameters, which the highest degradation efficiencies were obtained, was found as follows Initial Rh-B concentration: 10 ppm; Amount of catalyst: 15 mg/L; Reaction Temperature: 25 °C

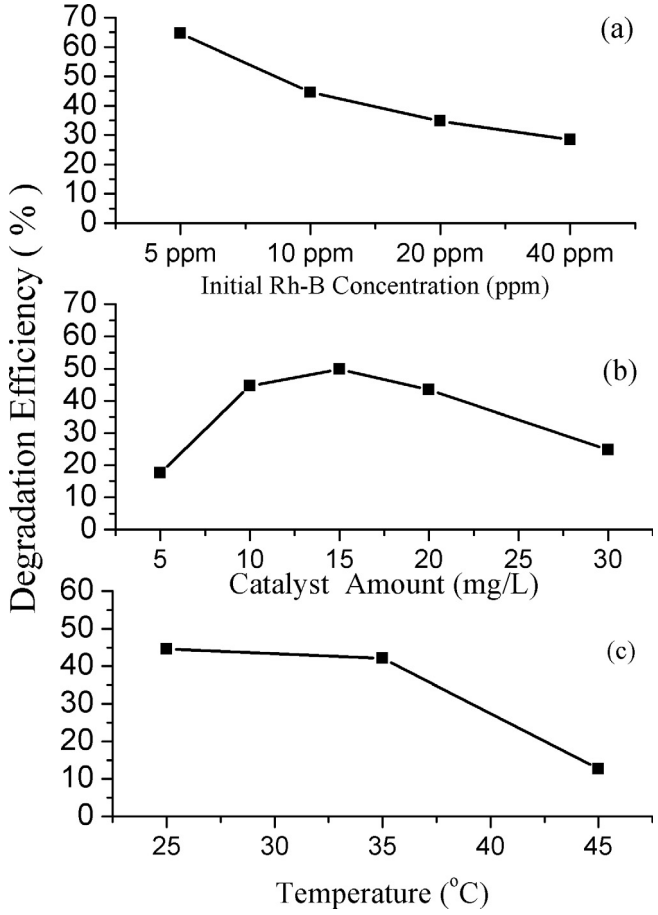

Fig. 5. Effect of Initial Rh-B concentration on degradation efficiency (a) (T = 25 °C; Amount of Catalyst = 10 mg/L; pH = 7) Effect of catalyst amount on degradation efficiency (b) (T = 25 °C; Initial Rh-B concentration = 10 ppm; pH = 7), Effect of temperature on degradation efficiency (c) (Amount of Catalyst = 10 mg/L; Initial Rh-B concentration = 10 ppm, pH = 7).

Another important parameter affected the degradation efficiency is pH of solution. The impact of pH of the solution on Rh-B degradation efficiency is shown in Fig. 6. Inset figure shows the change in degradation efficiency with respect to various solution pH at t = 90 min. As seen in figures, the degradation efficiency was found to be lower than the neutral conditions, in acidic (pH = 4) and basic (pH = 9) conditions. The effect of pH on sonocatalytic removal in the literature has been investigated in many studies. The change in the chemical behavior of the dye molecules and catalyst surface in acidic and basic conditions, has been shown to be an effective factor in degradation efficiency of the dye [39]. These results showed that, the surface charge of the catalyst at pH = 7, more appropriate than the that of in acidic and basic conditions.

In heterogeneous solid-liquid reaction systems, the reaction rate depends not only on the concentrations of the reagents but also on mass transfer mechanisms. The mechanism of the sonocatalytic oxidation in the literature is explained by two different hypotheses. According to the Langmuir-Hinshelwood heterogeneous reaction model, the reaction takes place on the catalyst surface. In this model dye molecules and reactive oxygen species firstly adsorbed on surface, then react on

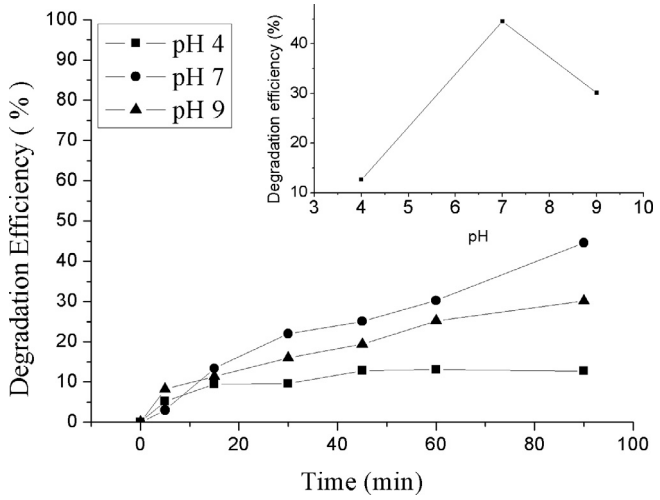

Fig. 6. Effect of pH of solution on degradation efficiency (T = 25 °C; Amount of Catalyst = 10 mg/L; Initial Rh-B concentration = 10 ppm).

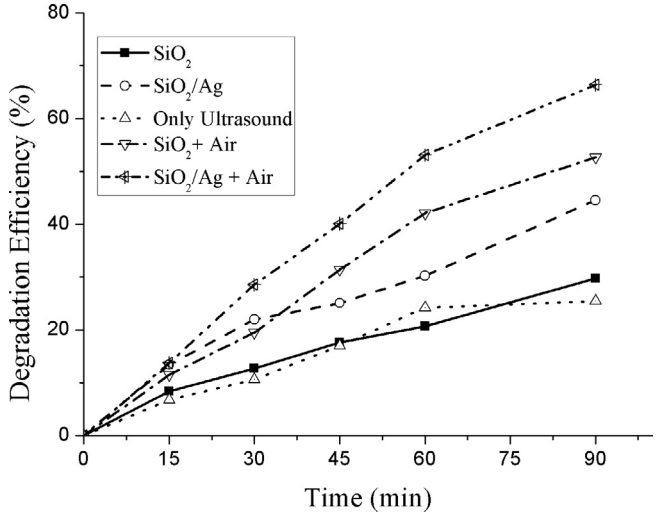

Fig. 7. Effect of O_2 saturation of solution on degradation efficiency (T = 25 °C; Amount of Catalyst = 10 mg/L; pH = 7 air flow = 0.6 L/min),

surface and finally products desorb from surface. Another approach in the literature assumes that the reaction takes place in bulk solution, not on the catalyst surface [40]. In this approach, the catalyst is only involved in the formation of reactive oxygen species. For both hypotheses, the reaction rate strongly dependent on amount of formed reactive oxygen species. At this point, it could be realistic to assume that, the actions promoted the formation of reactive oxygen species increase the degradation efficiency. To investigate the effect of O_2 saturation of solution and H_2O_2 addition to reaction on degradation efficiency, several experiments were performed while the other parameters were kept constant. Fig. 7 shows the obtained result to investigate effect of O_2 saturation of solution on degradation efficiency. In experiments without external O_2 source usage, it was observed that the maximum degradation efficiency was achieved in experiment which SiO_2/Ag Core/Shell nanoparticles was used as catalyst. Degradation efficiencies were found as 25.4%, 29.7%, 44.5% for only ultrasound, SiO_2 nanoparticles and SiO_2/Ag Core/Shell nanoparticles used experiments, respectively. This result indicate that the presence of Ag shell promoted the degradation efficiency. In the literature, publications on the use of silver compounds as sonocatalyst are limited. Zhang and coworkers investigated the sonocatalytic activity of Ag_3PO_4 and Br-Ag_3PO_4 for Rh-B, methylene blue and methyl orange degradation [41].

As seen in figure, degradation efficiencies of the experiments which the air was pumped through the solution, were higher than that of the experiments in which air was not pumped. It was reported that, dissolved gases behaved like nucleation points in solution during the ultrasonic cavitation [7]. Also it was reported that the some dissolved gases such as O_2 promote the reactive oxygen formation by decomposition of itself into radicals [42,43]. Synergetic effect between both presence of SiO_2/Ag Core/Shell nanoparticles and usage of external O_2 source, contributed the degradation efficiency and it was found as nearly 67% at the end of 90 min.

Oxidizing agents such as H_2O_2 are often added to the solution to increase the efficiency of sonocatalytic oxidation in literature. The formation enthalpy of the O–O bond in H_2O_2 structure is 213 kJ/mol while the formation enthalpy of the O–H bond in water molecule is 418 kJ/mol. In theory, it should be easier to break O–O bond in H_2O_2 structure than to break O–H bond in belong to water molecule. In literature, It was reported that the H_2O_2 decompose into •OH with the help of heat formed during the sonocatalytic cavitation, and improve the degradation efficiency [44]. To investigate the effect of H_2O_2 concentration on degradation efficiency, experiments were performed with different initial H_2O_2 concentrations (1, 5, 10, 20, 30, 40 and 50 mM) while the other parameters were kept constant. The degradation efficiencies obtained in experiments at the end of 90 min are illustrated in Fig. 8. The result showed that the addition of certain amount of H_2O_2 concentration proportionally increase the degradation efficiency but increase in H_2O_2 concentration higher than 10 mM had adverse effect on degradation efficiency. The degradation efficiencies were found as 49.7%, 54.3% and 56.7% for experiments which initial H_2O_2 concentrations was set as 1, 5, 10 mM, respectively. These obtained results were higher than the degradation efficiency of the experiment which the SiO_2/Ag Core/Shell nanoparticles used as catalyst without H_2O_2 usage (44.6%). In literature, there were several reports which parallel results were obtained. It has been reported that excessive use of H_2O_2 caused a reduction in degradation efficiency by the way of consumption of formed hydroxyl radicals [45]. The optimum amount of H_2O_2 varies depending on reaction conditions, such as temperature, pH, used catalyst and ultrasonic frequency etc.

Another important parameter to investigate the activity of the catalyst mostly employed in literature is Chemical Oxygen Demand (COD) value after experimental run. In our experiments, COD values were also tried to be determined, but obtained results did not show meaningful conclusions. These drawbacks were also reported in literature before.

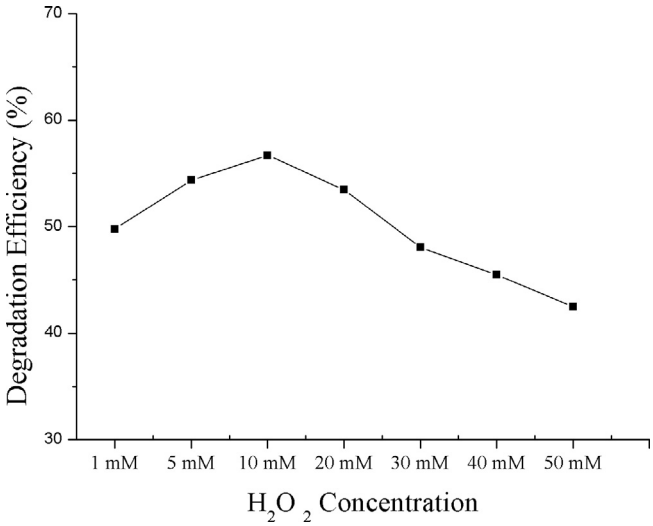

Fig. 8. Effect of H_2O_2 addition on degradation efficiency (T = 25 °C; Initial Rh-B concentration = 10 ppm; pH = 7; H_2O_2 concentrations = 1, 5, 10, 20, 30, 40 and 50 mM),

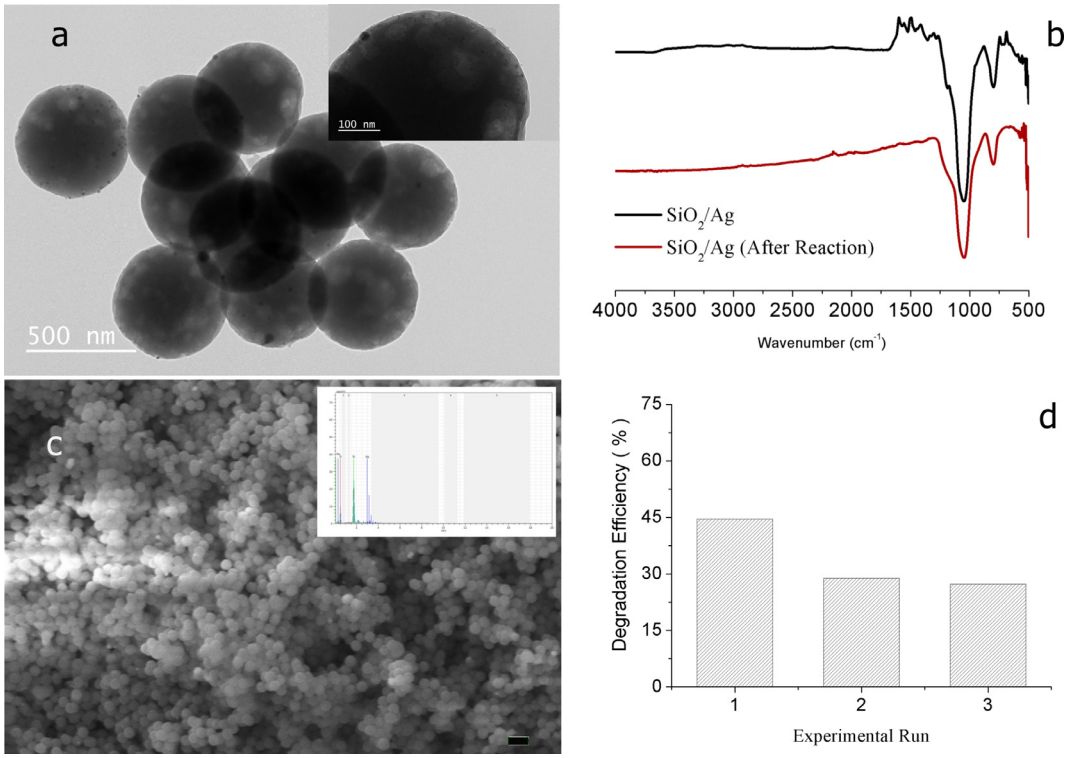

Fig. 9. The characterization results of spent catalyst: TEM images of spent SiO_2/Ag Core/Shell nanoparticles (a), ATR-FTIR spectrum of fresh and spent SiO_2/Ag Core/Shell nanoparticles (b), SEM image of spent SiO_2/Ag Core/Shell nanoparticles (c) (inset figure shows EDX spectra of spent catalyst; scale bar = 1 μm); The effect of re-usage of catalyst on degradation efficiency at t = 90 (d) (Amount of spent Catalyst = 10 mg/L; Initial Rh-B concentration = 10 ppm, pH = 7, T = 25 °C).

$Cr_2O_7^{-2}$ ion used in COD tests for reduction of organic molecules, is reduced with H_2O_2 formed during the ultrasonic cavitation and Cl^- ion belong to Rh-B structure [46]. These phenomena caused meaningless COD results in our experiments.

Stability of the catalyst is important factor that affect performance of catalyst in many applications. For investigating reusability of the SiO_2/Ag Core/Shell nanoparticles, several degradation experiments performed. Reusability experiment were performed by using spent catalyst several times with same conditions for ordinary degradation experiment. Also, the change in chemical composition and morphology of the SiO_2/Ag Core/Shell nanoparticles after reusability experiments was investigated by using TEM, SEM-EDX and FTIR techniques. The results of characterization of spent catalyst and reusability experiments are shown in Fig. 9 in an integrated manner. As seen in Fig. 9(d), degradation efficiency was decreased with the number of usages of catalyst. At the end of third usage, the obtained degradation efficiency (29.32%) nearly same with the uncoated samples (29.7%). It was thought that the activity loss could be originated from the surface erosion because of extreme conditions occurred during the collapse of the cavitation bubbles. It was reported that the shock waves formed during the collapse of cavitation bubbles could speed up solid particles in the liquid [27]. These high energetic particles could collide violently and may cause surface erosion. TEM images of spent SiO_2/Ag Core/Shell nanoparticles are seen in Fig. 9(a). As seen in Fig. 9(a) the although the particles preserved their spherical shape, the lighter area which corresponded to holes formed because of surface erosion could be seen. TEM images of spent catalyst with higher magnification is seen in inset figure. The erosion on surface could be seen more clearly in this image. The average particle size of spent catalyst was found as 502 ± 18 nm and this result were nearly same with the fresh catalyst. But it was obviously seen that the population of the incorporated Ag nanoparticles on surface of spent catalyst was lower than that of fresh catalyst. In Fig. 9(c) SEM image of spent SiO_2/Ag Core/Shell nanoparticles is seen. As seen in figure, all the particles were in spherical shape and equidimensional. There was no agglomeration seen in figure. EDX spectra of spent catalyst is seen in inset Fig. 9(c). The surface concentration of Ag was found as 3.49%. This value is lower than the result obtained for fresh catalyst (4.94%). In agreement with the TEM results, this result showed that, some of the Ag particles was removed from surface because of surface erosion. The decrease in population of Ag nanoparticles, especially larger particles, may lead to decrease in degradation efficiency. Another possible reason for decrease in degradation efficiency could be surface accumulation of side products formed during the oxidation of Rh-B. ATR-FTIR spectrum of spent catalyst is seen in Fig. 9(b). As seen in figure there was no additional peaks that is not belong to catalyst structure could be detected and both spectrum which were belong to fresh and spent catalyst, were identical.

4. Conclusions

Obtained results showed that the SiO_2/Ag Core/Shell nanoparticles appeared to be the active catalyst in degradation of Rh-B. To investigate the catalytic activity of SiO_2/Ag Core/Shell particles firstly optimum reaction conditions were determined. The optimum conditions were found as follows: catalyst amount = 15 mg/L; reaction temperature = 25 °C; Initial Rh-B concentration = 10 ppm. At these conditions the degradation efficiency was found as 49.6% at the end of 90 min. By keeping other parameters constant, the effect of pH of solution, O_2 saturation of solution and H_2O_2 addition to the solution on degradation efficiency were examined. It was indicated that the prepared SiO_2/Ag Core/Shell nanoparticles showed highest activity at pH = 7. Pumping air through the solution increased the degradation efficiency with the presence of SiO_2/Ag Core/Shell nanoparticle. Degradation efficiency was reached up to % 67 at the end of 90 min, for this experiment. Obtained results in this study showed that the addition of H_2O_2 contribute to the degradation efficiency in presence of SiO_2/Ag Core/Shell nanoparticle at certain initial concentration. But it was found that higher initial concentrations of H_2O_2 than 10 mM, had

adverse effects on degradation efficiency of Rh-B. Reusability of the SiO_2/Ag Core/Shell nanoparticle was also investigated in this study. Despite the reusability of the catalyst was found as limited, comparable activity of the catalyst even at low amount, make it good candidate for using it as catalyst in waste water treatment

Acknowledgement

Financial supports provided by the Mugla Sıtkı Koçman University with BAP project numbered 2013/16 are gratefully acknowledged.

Appendix A. Supplementary data

Supplementary data to this article can be found online at https://doi.org/10.1016/j.ultsonch.2018.10.025.

References

[1] M. Dükkancı, M. Vinatoru, T.J. Mason, The sonochemical decolourisation of textile azo dye Orange II: effects of Fenton type reagents and UV light, Ultrason. Sonochem. 21 (2014) 846–853, https://doi.org/10.1016/j.ultsonch.2013.08.020.
[2] V.M. Correia, T. Stephenson, S.J. Judd, Characterisation of textile wastewaters – a review, Environ. Technol. 15 (1994) 917–929, https://doi.org/10.1080/09593339409385500.
[3] I. Bisschops, H. Spanjers, Literature review on textile wastewater characterisation, Environ. Technol. 24 (2003) 1399–1411, https://doi.org/10.1080/09593330309385684.
[4] J. Madhavan, P.S. Sathish Kumar, S. Anandan, F. Grieser, M. Ashokkumar, Degradation of acid red 88 by the combination of sonolysis and photocatalysis, Sep. Purif. Technol. 74 (2010) 336–341, https://doi.org/10.1016/j.seppur.2010.07.001.
[5] J. Madhavan, P.S. Sathish Kumar, S. Anandan, F. Grieser, M. Ashokkumar, Sonophotocatalytic degradation of monocrotophos using TiO_2 and Fe^{3+}, J. Hazard. Mater. 177 (2010) 944–949, https://doi.org/10.1016/j.jhazmat.2010.01.009.
[6] S.G. Anju, S. Yesodharan, E.P. Yesodharan, Zinc oxide mediated sonophotocatalytic degradation of phenol in water, Chem. Eng. J. 189–190 (2012) 84–93, https://doi.org/10.1016/j.cej.2012.02.032.
[7] L.H. Thompson, L.K. Doraiswamy, Sonochemistry: science and engineering, Ind. Eng. Chem. Res. 38 (1999) 1215–1249, https://doi.org/10.1021/ie9804172.
[8] Y.L. Pang, A.Z. Abdullah, S. Bhatia, Effect of annealing temperature on the characteristics, sonocatalytic activity and reusability of nanotubes TiO_2 in the degradation of Rhodamine B, Appl. Catal. B Environ. 100 (2010) 393–402, https://doi.org/10.1016/j.apcatb.2010.08.016.
[9] J. Wang, T. Ma, Z. Zhang, X. Zhang, Y. Jiang, Z. Pan, F. Wen, P. Kang, P. Zhang, Investigation on the sonocatalytic degradation of methyl orange in the presence of nanometer anatase and rutile TiO_2 powders and comparison of their sonocatalytic activities, Desalination 195 (2006) 294–305, https://doi.org/10.1016/j.desal.2005.12.007.
[10] J. Wang, Z. Jiang, Z. Zhang, Y. Xie, Y. Lv, J. Li, Y. Deng, X. Zhang, Study on inorganic oxidants assisted sonocatalytic degradation of Acid Red B in presence of nano-sized ZnO powder, Sep. Purif. Technol. 67 (2009) 38–43, https://doi.org/10.1016/j.seppur.2009.03.005.
[11] Y.L. Pang, A.Z. Abdullah, S. Bhatia, Review on sonochemical methods in the presence of catalysts and chemical additives for treatment of organic pollutants in wastewater, Desalination 277 (2011) 1–14, https://doi.org/10.1016/j.desal.2011.04.049.
[12] L. Zhang, R. Liu, H. Yang, Preparation and sonocatalytic activity of monodisperse porous bread-like CuO via thermal decomposition of copper oxalate precursors, Phys. E Low-Dimens. Syst. Nanostruct. 44 (2012) 1592–1597, https://doi.org/10.1016/j.physe.2012.04.001.
[13] Y. Wang, D. Zhao, W. Ma, C. Chen, J. Zhao, Enhanced sonocatalytic degradation of azo dyes by Au/TiO_2, Environ. Sci. Technol. 42 (2008) 6173–6178 http://www.ncbi.nlm.nih.gov/pubmed/18767683.
[14] J. Wang, Y. Lv, Z. Zhang, Y. Deng, L. Zhang, B. Liu, R. Xu, X. Zhang, Sonocatalytic degradation of azo fuchsine in the presence of the Co-doped and Cr-doped mixed crystal TiO_2 powders and comparison of their sonocatalytic activities, J. Hazard. Mater. 170 (2009) 398–404, https://doi.org/10.1016/j.jhazmat.2009.04.083.
[15] N. Ghows, M.H. Entezari, Exceptional catalytic efficiency in mineralization of the reactive textile azo dye (RB5) by a combination of ultrasound and core – shell nanoparticles (CdS/TiO_2), J. Hazard. Mater. 195 (2011) 132–138, https://doi.org/10.1016/j.jhazmat.2011.08.049.
[16] H. Salavati, N. Tavakkoli, M. Hosseinpoor, Preparation and characterization of polyphosphotungstate/ZrO_2 nanocomposite and their sonocatalytic and photocatalytic activity under UV light illumination, Ultrason. Sonochem. 19 (2012) 546–553, https://doi.org/10.1016/j.ultsonch.2011.09.001.
[17] J. Wang, Z. Pan, Z. Zhang, X. Zhang, Y. Jiang, T. Ma, F. Wen, Y. Li, P. Zhang, The investigation on ultrasonic degradation of acid fuchsine in the presence of ordinary and nanometer rutile TiO_2 and the comparison of their sonocatalytic activities, Dye Pigment 74 (2007) 525–530, https://doi.org/10.1016/j.dyepig.2006.03.010.
[18] H. Chen, S. Liu, J. Wang, D. Chen, Study on effect of microparticle's size on cavitation erosion in solid-liquid system, J. Appl. Phys. 101 (2007) 103510, , https://doi.org/10.1063/1.2734547.
[19] B. Sambandam, V. Soundharrajan, J. Song, S. Kim, J. Jo, D.T. Pham, S. Kim, V. Mathew, K.H. Kim, Y.K. Sun, J. Kim, $Ni_3V_2O_8$ nanoparticles as an excellent anode material for high-energy lithium-ion batteries, J. Electroanal. Chem. 810 (2018) 34–40, https://doi.org/10.1016/j.jelechem.2017.12.083.
[20] M. Ghiyasiyan-Arani, M. Salavati-Niasari, Effect of $Li_2CoMn_3O_8$ nanostructures synthesized by a combustion method on montmorillonite K10 as a potential hydrogen storage material, J. Phys. Chem. C 122 (2018) 16498–16509, https://doi.org/10.1021/acs.jpcc.8b02617.
[21] A. Salehabadi, M. Salavati-Niasari, M. Ghiyasiyan-Arani, Self-assembly of hydrogen storage materials based multi-walled carbon nanotubes (MWCNTs) and $Dy_3Fe_5O_{12}$(DFO) nanoparticles, J. Alloys Compd. 745 (2018) 789–797, https://doi.org/10.1016/j.jallcom.2018.02.242.
[22] F. Soofivand, F. Mohandes, M. Salavati-Niasari, Silver chromate and silver dichromate nanostructures: sonochemical synthesis, characterization, and photocatalytic properties, Mater. Res. Bull. 48 (2013) 2084–2094, https://doi.org/10.1016/j.materresbull.2013.02.025.
[23] N. Kumar, R. Bogireddy, H. Anand, K. Kumar, B.K. Mandal, Biofabricated silver nanoparticles as green catalyst in the degradation of different textile dyes, J. Environ. Chem. Eng. 4 (2016) 56–64, https://doi.org/10.1016/j.jece.2015.11.004.
[24] C. Min, J. Heo, Y. Yoon, Oxidative degradation of bisphenol A and 17 a-ethinyl estradiol by Fenton-like activity of silver nanoparticles in aqueous solution, Chemosphere 168 (2017) 617–622, https://doi.org/10.1016/j.chemosphere.2016.11.016.
[25] D. He, C.J. Miller, T.D. Waite, Fenton-like zero-valent silver nanoparticle-mediated hydroxyl radical production, J. Catal. 317 (2014) 198–205, https://doi.org/10.1016/j.jcat.2014.06.016.
[26] M. Masjedi-arani, M. Salavati-niasari, D. Ghanbari, G. Nabiyouni, A sonochemical-assisted synthesis of spherical silica nanostructures by using a new capping agent, Ceram. Int. 40 (2014) 495–499, https://doi.org/10.1016/j.ceramint.2013.06.029.
[27] R. Monsef, M. Ghiyasiyan-Arani, M. Salavati-Niasari, Application of ultrasound-aided method for the synthesis of $NdVO_4$ nano-photocatalyst and investigation of eliminate dye in contaminant water, Ultrason. Sonochem. 42 (2018) 201–211, https://doi.org/10.1016/j.ultsonch.2017.11.025.
[28] M. Ghiyasiyan-Arani, M. Salavati-Niasari, S. Naseh, Enhanced photodegradation of dye in waste water using iron vanadate nanocomposite; ultrasound-assisted preparation and characterization, Ultrason. Sonochem. 39 (2017) 494–503, https://doi.org/10.1016/j.ultsonch.2017.05.025.
[29] M. Ghiyasiyan-Arani, M. Salavati-Niasari, M. Masjedi-Arani, F. Mazloom, An easy sonochemical route for synthesis, characterization and photocatalytic performance of nanosized $FeVO_4$ in the presence of aminoacids as green capping agents, J. Mater. Sci. Mater. Electron. 29 (2018) 474–485, https://doi.org/10.1007/s10854-017-7936-9.
[30] F. Mohandes, M. Salavati-Niasari, Sonochemical synthesis of silver vanadium oxide micro/nanorods: solvent and surfactant effects, Ultrason. Sonochem. 20 (2013) 354–365, https://doi.org/10.1016/j.ultsonch.2012.05.002.
[31] M. Goudarzi, N. Mir, M. Mousavi-Kamazani, S. Bagheri, M. Salavati-Niasari, Biosynthesis and characterization of silver nanoparticles prepared from two novel natural precursors by facile thermal decomposition methods, Sci. Rep. 6 (2016) 32539, https://doi.org/10.1038/srep32539.
[32] K.S. Rao, K. El-Hami, T. Kodaki, K. Matsushige, K. Makino, A novel method for synthesis of silica nanoparticles, J. Colloid Interface Sci. 289 (2005) 125–131, https://doi.org/10.1016/j.jcis.2005.02.019.
[33] Y. Zhu, X. Wang, W. Guo, J. Wang, C. Wang, Sonochemical synthesis of silver nanorods by reduction of silver nitrate in aqueous solution, Ultrason. Sonochem. 17 (2010) 675–679, https://doi.org/10.1016/j.ultsonch.2010.01.003.
[34] T. Gholami, M. Salavati-niasari, M. Bazarganipour, Superlattices and microstructures synthesis and characterization of spherical silica nanoparticles by modified Stöber process assisted by organic ligand, Superlattices Microstruct. 61 (2013) 33–41, https://doi.org/10.1016/j.spmi.2013.06.004.
[35] C.-K. Huang, C.-Y. Chen, J.-L. Han, C.-C. Chen, M.-D. Jiang, J.-S. Hsu, C.-H. Chan, K.-H. Hsieh, Immobilization of silver nanoparticles on silica microspheres, J. Nanoparticle Res. 12 (2009) 199–207, https://doi.org/10.1007/s11051-009-9594-1.
[36] J. Wang, Z. Jiang, Z. Zhang, Y. Xie, X. Wang, Z. Xing, R. Xu, X. Zhang, Sonocatalytic degradation of acid red B and rhodamine B catalyzed by nano-sized ZnO powder under ultrasonic irradiation, Ultrason. Sonochem. 15 (2008) 768–774, https://doi.org/10.1016/j.ultsonch.2008.02.002.
[37] M. Geng, S.M. Thagard, Ultrasonics sonochemistry the effects of externally applied pressure on the ultrasonic degradation of Rhodamine B, Ultrason. Sonochem. 20 (2013) 618–625, https://doi.org/10.1016/j.ultsonch.2012.08.002.
[38] M. Zhou, H. Yang, T. Xian, R.S. Li, H.M. Zhang, X.X. Wang, Sonocatalytic degradation of RhB over $LuFeO_3$ particles under ultrasonic irradiation, J. Hazard. Mater. 289 (2015) 149–157, https://doi.org/10.1016/j.jhazmat.2015.02.054.
[39] N.H. Ince, G. Tezcanli-Güyer, Impacts of pH and molecular structure on ultrasonic degradation of azo dyes, Ultrasonics 42 (2004) 591–596, https://doi.org/10.1016/j.ultras.2004.01.097.
[40] S. Vajnhandl, A.M. Le Marechal, Case study of the sonochemical decolouration of textile azo dye Reactive Black 5, J. Hazard. Mater. 141 (2007) 329–335, https://doi.org/10.1016/j.jhazmat.2006.07.005.
[41] P. He, L. Song, X. Wu, H. Tian, Q. Wei, J. Ye, L. Zhang, Y. Cui, Y. Wang, Fabrication and sonocatalytic property of $AgPO_3$ microsphere, Ultrason. Sonochem. 21 (2014) 136–141, https://doi.org/10.1016/j.ultsonch.2013.07.017.
[42] Y.G. Adewuyi, Sonochemistry in environmental remediation. 2. Heterogeneous sonophotocatalytic oxidation processes for the treatment of pollutants in water, Environ. Sci. Technol. 39 (2005) 8557–8570 http://www.ncbi.nlm.nih.gov/

pubmed/16323748.
[43] T. Chave, N.M. Navarro, P. Pochon, N. Perkas, A. Gedanken, S.I. Nikitenko, Sonocatalytic degradation of oxalic acid in the presence of oxygen and Pt/TiO_2, Catal. Today 241 (2015) 55–62, https://doi.org/10.1016/j.cattod.2014.07.040.
[44] Y.L. Pang, S. Bhatia, A.Z. Abdullah, Process behavior of TiO_2 nanotube-enhanced sonocatalytic degradation of Rhodamine B in aqueous solution, Sep. Purif. Technol. 77 (2011) 331–338, https://doi.org/10.1016/j.seppur.2010.12.023.
[45] M. Abbasi, N.R. Asl, Sonochemical degradation of Basic Blue 41 dye assisted by nanoTiO_2 and H_2O_2, J. Hazard. Mater. 153 (2008) 942–947, https://doi.org/10.1016/j.jhazmat.2007.09.045.
[46] Y.L. Pang, A.Z. Abdullah, S. Bhatia, Optimization of sonocatalytic degradation of Rhodamine B in aqueous solution in the presence of TiO_2 nanotubes using response surface methodology, Chem. Eng. J. 166 (2011) 873–880, https://doi.org/10.1016/j.cej.2010.11.059.